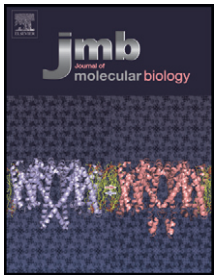

Sum of the Parts: Composition and Architecture of the Bacterial Extracellular Matrix

Oscar A. McCrate†, Xiaoxue Zhou†, Courtney Reichhardt and Lynette Cegelski

Department of Chemistry, *Stanford University, Stanford, CA 94305, USA*

Correspondence to Lynette Cegelski: *cegelski@stanford.edu*
http://dx.doi.org/10.1016/j.jmb.2013.06.022
Edited by M. F. Summers

Abstract

Bacterial biofilms are complex multicellular assemblies that exhibit resistance to antibiotics and contribute to the pathogenesis of serious and chronic infectious diseases. New approaches and quantitative data are needed to define the molecular composition of bacterial biofilms. *Escherichia coli* biofilms are known to contain polysaccharides and functional amyloid fibers termed curli, yet accurate determinations of biofilm composition at the molecular level have been elusive. The ability to define the composition of the extracellular matrix (ECM) is crucial for the elucidation of structure–function relationships that will aid the development of chemical strategies to disrupt biofilms. We have developed an approach that integrates non-perturbative preparation of the ECM with electron microscopy, biochemistry, and solid-state NMR spectroscopy to define the chemical composition of the intact and insoluble ECM of a clinically important pathogenic bacterium—uropathogenic *E. coli*. Our data permitted a sum-of-all-the-parts analysis. Electron microscopy revealed supramolecular shell-like structures that encapsulated single cells and enmeshed the bacterial community. Biochemical and solid-state NMR measurements of the matrix and constitutive parts established that the matrix is composed of two major components, curli and cellulose, each in a quantifiable amount. This approach to quantifying the matrix composition is widely applicable to other organisms and to examining the influence of biofilm inhibitors. Collectively, our NMR spectra and the electron micrographs of the purified ECM inspire us to consider the biofilm matrix not as an undefined slime, but as an assembly of polymers with a defined composition and architecture.

Introduction

Bacterial biofilms are multicellular assemblies, characterized by a complex extracellular polymeric matrix that can include proteins, polysaccharides, lipids, and nucleic acids. The propensity for bacteria to exist in biofilm communities in the biosphere far exceeds the tendency for bacteria to persist as individual planktonic cells. Biofilms are essential to life in terrestrial and aquatic habitats but are also associated with adverse consequences such as biofouling and disease [1–4]. Indeed, biofilm bacteria can exhibit reduced sensitivity to antibiotics and host defenses and have emerged as hallmarks of serious and persistent infectious diseases, including cystic fibrosis pneumonia, infective endocarditis, urinary tract infection, periodontitis, chronic otitis media, and infections of medical devices such as intravenous catheters and artificial joints [5,6]. Currently available antibiotics often fail to eradicate biofilm-associated bacteria, necessitating multiple and intense antibiotic treatment regimens that can exhaust the pool of last-resort antibiotics [5,7]. As a consequence, biofilm-associated infections are the cause of significant morbidity and mortality in the clinic. New therapeutic strategies are needed to prevent and eradicate biofilms [5–7]. An improved understanding of biofilm composition and function is crucial to understanding the modes of action of candidate biofilm inhibitors and driving the development of new strategies to target biofilm formation.

Important genetic and molecular determinants of biofilm formation have been elucidated in some systems, with many matrix components having been identified by techniques such as mass spectrometry, immunochemistry, and microscopy [8]. However,

formidable challenges exist in generating a complete accounting of the parts and in understanding how the parts assemble and function [9]. Analyses of biofilm composition by standard methods often employ harsh hydrolysis protocols coupled with mass spectrometry [10]. This degradative approach is complicated by incomplete dissolution as well as the perturbative nature of chemical and enzymatic processing.

We have developed an approach that integrates minimally perturbative preparation of extracellular matrix (ECM) material, biochemical characterization of the ECM, and solid-state NMR spectroscopy to define the composition of the ECM. We selected the clinically relevant uropathogenic *Escherichia coli* strain UTI89, which is known to produce at least curli amyloid fibers and cellulose in its ECM, to establish our methodology and to define the biofilm composition of an important human pathogen. Curli were discovered to be amyloid in 2002 [11] and an increasing number of functional amyloid fibers are being identified in other bacteria [12–15]. From detailed studies in *E. coli*, *Salmonella*, *Bacillus subtilis*, and *Staphylococcus aureus*, microorganisms harness the amyloid-forming pathway to assemble functional adhesive fibers that contribute to cellular physiology, adhesion, and biofilm formation [15–19]. Thus, there is great interest in understanding how the integration of amyloids in biofilms influences biofilm composition and function. Biofilm formation and curli production have been implicated in the pathogenesis of urinary tract infection [20–22], and approaches to quantify biofilm composition in uropathogenic *E. coli* will be of tremendous value in examining the differences in virulence and pathogenesis of different uropathogenic *E. coli* and other pathogenic bacteria. Indeed, *E. coli* can form many types of biofilms, integrating different extracellular fimbriae depending on the growth conditions [23,24]. When grown on YESCA nutrient agar, UTI89 forms an amyloid-based biofilm consisting of curli amyloid fibers, cellulose, and potentially other components, although the exact composition of such biofilms has not been defined [20,48]. The co-requirement for cellulose during biofilm formation has been ascribed to the presence of and requirement of cellulose synthase genes and the detection of glucose in hydrolyzed ECM samples, coupled with the ability to stain biofilms with the dye calcofluor and to disrupt biofilms using cellulase [10,23,25,26]. However, the quantification of cellulose content relative to other ECM components, or the possibility of having a modified form of cellulose in the ECM, has not been determined.

UTI89 assembles a biofilm that exhibits the hallmark wrinkled colony morphology associated with both *E. coli* and *Salmonella* strains when grown under curli- and cellulose-producing conditions, such as on YESCA nutrient agar [27]. Congo red is often included in the nutrient agar to visually emphasize the colony morphology, referred to as the red, dry, and rough phenotype [10]. Congo red can bind to both curli and cellulose and is used to qualitatively distinguish different types of biofilm formers [10,25]. We recently reported that curcumin also binds to curli and can be used as an amyloid-specific dye [28]. Another commonly employed dye, calcofluor white, binds to polysaccharides and is used to score the production of cellulose and other possible polysaccharides in the biofilm matrix [10,25]. Such dyes are useful as they can be used within the context of intact, unperturbed biofilm samples. However, they provide only qualitative information regarding biofilm composition.

Solid-state NMR is nondestructive and uniquely suited to examine the chemical composition and structure of complex and insoluble biomaterials including whole cells, bacterial cell walls, intact soybean leaves, and insect cuticle [29–32]. We have obtained ^{13}C cross-polarization magic-angle spinning (CPMAS) NMR spectra of the purified ECM from UTI89 and of isolated biofilm components, characterized each of these biochemically and spectroscopically, and discovered that this yielded a quantitative determination of the composition of the insoluble ECM.

Results

The ECM in UTI89 biofilm forms a robust, well-ordered network encapsulating single cells

A biofilm is composed of bacterial cells plus their ECM. To examine the composition of the ECM, we developed an ECM extraction protocol, based on the curli isolation protocol of Chapman *et al.* [11], to remove the matrix material from the intact cells. We found that Congo red, commonly used during growth as an indicator dye of ECM production, was useful for tracking the purification, as it binds to both curli and cellulose, and serves as a precipitation agent for polysaccharide purification as previously recognized [33]. Thus, the ECM samples were prepared from bacteria grown in the presence of Congo red.

We examined preparations of the intact wild-type UTI89 ECM; the ECM material from the curli mutant, UTI89Δ*csgA* [20]; and intact curli produced by the laboratory strain MC4100. MC4100 does not produce cellulose and is used extensively in studies of *E. coli* curli biogenesis and for the isolation of curli fibers [11]. We compared the purified material from these strains with their non-perturbed whole-cell counterparts by electron microscopy. Scanning electron micrographs revealed extensive long-range connectivity, encapsulation, and network formation among UTI89 cells in a biofilm, whereas the cells in

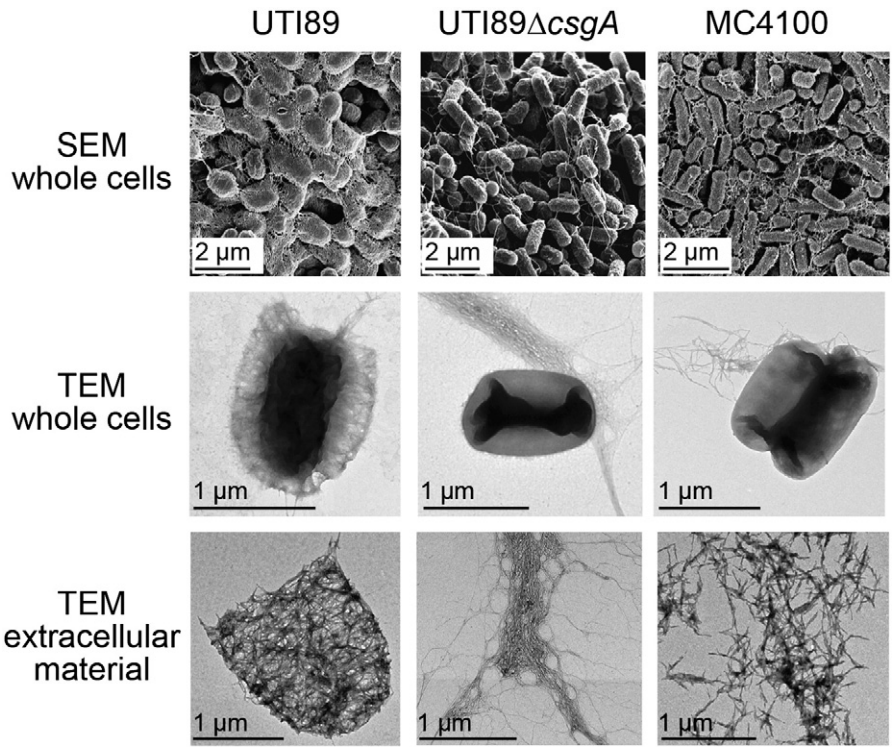

Fig. 1. Electron micrograph comparisons of whole cells [scanning electron microscopy (SEM), top row, and transmission electron microscopy (TEM), middle row] of UTI89, UTI89Δ*csgA*, and MC4100, and the extracted extracellular material (TEM, bottom row) from each strain. SEM images were obtained from intact single colonies grown on YESCA agar. TEM images were obtained from bacteria resuspended in Tris buffer following growth on agar.

the UTI89Δ*csgA* sample are separated from one another, exhibiting only loose connections (Fig. 1). MC4100 cells are also well separated from one another, but exhibit some intercellular connectivity through curli fibers (Fig. 1).

Transmission electron micrographs of whole-cell samples revealed shell-like structures surrounding individual UTI89 cells that retained their shape even after mechanical disruption and separation of the ECM (Fig. 1). In contrast, the curli mutant, UTI89 Δ*csgA*, exhibited no remarkable organization with extracellular material being loosely cell-associated (Fig. 1). Similarly, curli fibers are loosely cell-associated without considerable organization in MC4100 samples (Fig. 1).

Curli comprise the major protein component in the UTI89 ECM

With the ability to extract the extracellular material from our three strains, we sought to determine whether non-curli proteins also contribute to the composition of the UTI89 biofilm and whether such potential proteins might be part of the insoluble biofilm matrix or only loosely associated with it. To do this, we analyzed the isolated extracellular extracts from UTI89, UTI89Δ*csgA*, and MC4100 by SDS-PAGE.

Curli and other amyloid fibers are not denatured by boiling in SDS and require strong solvents such as concentrated formic acid or hexafluoroisopropanol for depolymerization [11,34]. Thus, the purified ECM and comparative samples were treated with 88% formic acid to depolymerize the curli fibers, followed by vacuum centrifugation to remove the solvent before resuspending samples in protein sample buffer. The non-SDS-washed UTI89 ECM exhibits three major protein bands by SDS-PAGE (Fig. 2) identified by Western blot analysis and/or Edman degradation as CsgA at 16 kDa, CsgA dimer at 34 kDa, and FliC, the main structural protein of the flagellum, at 60 kDa. Flagella have been observed in curli-associated biofilms [48]. Under heavy loading, additional bands could be detected in the non-SDS-washed samples, although they were present at very low abundance and were not present in all isolations (Fig. 2). We hypothesized that these could be attributed to weakly associated proteins that may have remained with the ECM adventitiously. Mass spectrometry analysis confirmed that the bands were cell-membrane-associated proteins, including the following: EF-Tu, elongation factor Tu; TF, trigger factor; PflB, formate acetyltransferase 1; and AdhE, aldehyde-alcohol dehydrogenase [35]. Washing of the UTI89 ECM in 4% SDS removed FliC and the low abundance bands, indicating that these proteins are

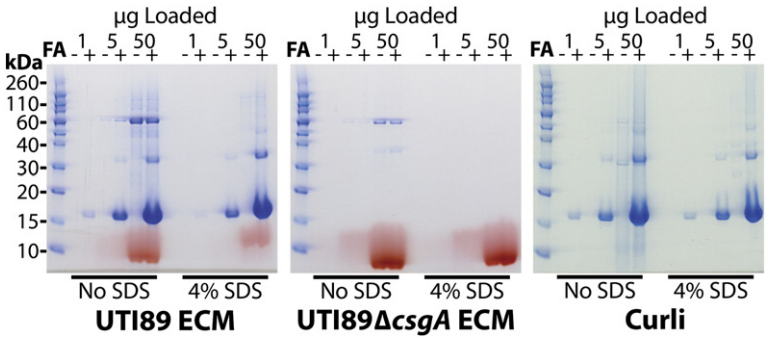

Fig. 2. SDS-PAGE comparison of the extracted ECM from UTI89, the cellulose-containing extracellular material from UTI89Δ*csgA*, and curli from MC4100. Protein gels reveal the proteins present in each sample before and after incubation with 4% SDS. Each sample was run with and without formic acid (FA) treatment to enable the comparison of SDS-soluble proteins with the curli fiber subunit, CsgA, which is SDS-resistant but FA-soluble. Gels were incubated in 1.25 M Tris buffer (pH 8.8) to distinguish Congo red from Coomassie blue.

not part of the intrinsically insoluble ECM (Fig. 2). Collectively, our data demonstrate that curli are overwhelmingly the major protein component of the insoluble ECM produced when UTI89 is grown on YESCA nutrient agar.

Gels corresponding to the UTI89Δ*csgA* extracellular material were cleaner with fewer proteins detected (Fig. 2). This could be attributed to the weaker association with the UTI89Δ*csgA* extracellular material (Fig. 2) in the absence of curli, which are adhesive fibers, resulting in fewer proteins being pulled away from the cells during the extraction. For the non-SDS-washed UTI89Δ*csgA* ECM, only three protein bands were observed: OmpA at 38 kDa, OmpF and OmpC at 39 kDa, and FliC at 60 kDa. As anticipated, no CsgA was observed in UTI89Δ*csgA*. Additionally, washing the UTI89Δ*csgA* ECM in 4% SDS removed FliC and the outer membrane protein bands, whereas curli remain tightly associated with the SDS-treated ECM.

The SDS-PAGE gels of curli isolated from MC4100 exhibited the typical array of curli protein bands (Fig. 2). Curli fibers are composed of the protein CsgA and, as expected, the gel shows one major band present after formic acid treatment at 16 kDa corresponding to the CsgA monomer, with additional bands present at approximately 32 and 50 kDa corresponding to the CsgA dimer and trimer, respectively (Fig. 2) [11].

The UTI89Δ*csgA* ECM harbors a modified form of cellulose

The polysaccharide component of the UTI89 ECM is expected to contain cellulose. Thus, in the curli mutant, we anticipated that we would observe carbon contributions from CR, cellulose, and potentially other components. We compared the UTI89 Δ*csgA* ECM spectrum to the ^{13}C CPMAS spectra of equal masses of commercially available cellulose and Congo red (Fig. 3). The UTI89Δ*csgA* ECM spectrum harbors carbon contributions from cellulose and Congo red in approximately a one-to-one ratio (Fig. 3). The absence of a carbonyl peak (~175 ppm) and the lack of additional peaks in the protein aliphatic region indicate that there are no proteins or amino acids in the sample, consistent with the protein gel analysis. Differences in the lineshapes between the commercially purchased crystalline powders and the biological sample are expected due to differences in the molecular conformations, packing, and environment of the two samples [36]. The UTI89Δ*csgA* ECM chemical shifts are also consistent with the presence of cellulose in biological samples [37,38] and are not compatible with other abundant polysaccharides commonly associated with bacterial cells, including MurNAc, GlcNAc, lipopolysaccharide, or other

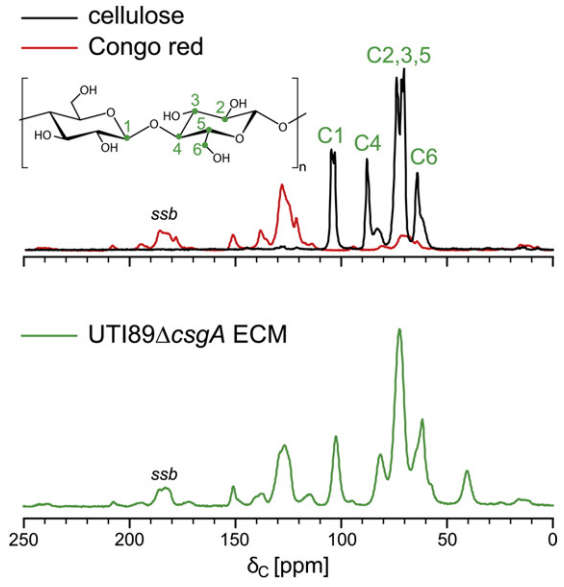

Fig. 3. ^{13}C CPMAS spectra of commercial cellulose and CR (top) compared with the extracellular material of the curli mutant strain, UTI89Δ*csgA*. The CR and cellulose spectra were scaled by mass and indicate that the CR contribution to the UTI89Δ*csgA*, centered at 128 ppm with its spinning sidebands, is 50%. MAS was performed at 7143 Hz, and 32,768 scans were obtained for each spectrum.

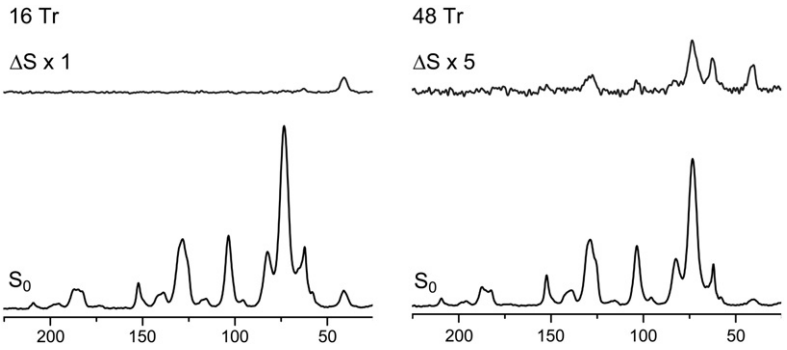

Fig. 4. $^{13}C\{^{15}N\}$ REDOR NMR spectra of uniformly ^{15}N-labeled UTI89Δ*csgA*. Nearly complete dephasing ($\Delta S/S_0$) of the 40-ppm carbon after the 16 Tr REDOR experiment with 7143-kHz MAS identifies this carbon as having a directly bonded nitrogen. Dephasing at longer evolution time reveals the proximity of the amino modification to other carbons at 62 and 74 ppm and to Congo red at 129 ppm. Each S_0 and S spectrum was the result of 40,960 scans for 16 Tr and 51,200 scans for 48 Tr.

carboxylated O- or K-antigens [39]. Interestingly, the presence of an additional carbon peak, centered at 40 ppm, was not accounted for in the commercially obtained crystalline cellulose or Congo red reference spectra.

Based on all the observed chemical shifts, we hypothesized that the 40-ppm chemical shift could be attributed to a cellulose modification that includes an $-OCH_2CH_2NH_3^+$ moiety, consistent with the chemical shift of the ε-carbon in lysine, but without other resonances observed upfield of it. An $-OCH_2NH_3^+$ would not be chemically stable and the absence of any carbonyl contribution eliminated the possibility of an acyl modification. To test our hypothesis, we uniformly ^{15}N labeled the UTI89Δ*csgA* ECM, using an optimized defined agar labeling medium that permits biofilm production in UTI89, and performed rotational-echo double-resonance (REDOR) [40] NMR to measure whether the 40-ppm carbon was directly bonded to a nitrogen. REDOR provides access to dipolar couplings that are averaged during magic-angle spinning (MAS) and is often used as a spectroscopic filter to select pairs of nuclei within a desired distance range [29]. The sample exhibited only a single peak in the ^{15}N CPMAS spectrum centered at 4.5 ppm, consistent with the proposed primary amine functionality. A 16-rotor cycle $^{13}C\{^{15}N\}$ REDOR experiment was performed to identify directly bonded $^{13}C-^{15}N$ pairs (Fig. 4). The 40-ppm carbon peak was nearly completely dephased, indicating that it is directly bonded to the single nitrogen detected in the ^{15}N CPMAS spectrum. After a 48-rotor cycle REDOR experiment, corresponding to 6.72 ms of evolution time, dephasing to other carbons was observed. Both the C6 carbon and the $-OCH_2CH_2NH_3^+$ carbon would appear near 62 ppm [41]. Thus, the REDOR data and the carbon chemical shifts indicate that the ^{15}N that is directly bonded to the 40-ppm carbon is next closest to a carbon or carbons at 62 ppm and then within detectable proximity to the other carbons in cellulose, suggestive of a hydroxyl-substituted O-linked 2-aminoethyl modification to cellulose.

Determination of the curli-to-polysaccharide ratio in the amyloid-integrated UTI89 ECM

The ultimate goal of our work was to define and quantify the contributions of curli and cellulose to the insoluble UTI89 ECM. Thus, we obtained and compared ^{13}C CPMAS spectra of the isolated UTI89 ECM, the cellulose-containing UTI89Δ*csgA* ECM, and curli purified from MC4100. All of the matrix components were SDS-washed to remove loosely associated proteins after extraction from whole cells and to determine the composition of the insoluble and intractable matrix material. The UTI89 Δ*csgA* ECM ^{13}C CPMAS spectrum, as described above, contains no detectable protein content, evidenced by the lack of a carbonyl peak at around 175 ppm, whereas the curli spectrum exhibits the typical qualities of a protein spectrum (Fig. 5). The curli NMR spectrum corresponds to a curli sample prepared from MC4100 grown on YESCA agar in the absence of CR as we demonstrated separately that SDS treatment removes CR from curli when prepared from cells grown on CR-containing YESCA (Fig. S1). Thus, the curli-only NMR spectrum does not harbor contributions from CR. A simple sum of the scaled curli and UTI89Δ*csgA* ECM spectra recapitulates the ^{13}C CPMAS spectrum of the UTI89 ECM (Fig. 5). The spectral sum resulted from normalizing each spectrum according to its mass and then scaling the intensity of the curli spectrum to 72% and that of the UTI89Δ*csgA*, CR-containing spectrum, to 28%. Thus, taking into account the percentage of Congo red in the sample (half of the UTI89Δ*csgA* spectrum), the curli:cellulose:CR contributions in the UTI89 ECM are 72:14:14. Excluding the CR contribution, the ECM contains curli and polysaccharide in approximately a 6:1 ratio (84% curli and 16% cellulose). In order to assess the impact of biological variability on this determination, we performed the ECM extraction and NMR analysis from cells grown months after the first preparation using separately prepared medium and bacterial starter cultures. This ECM preparation

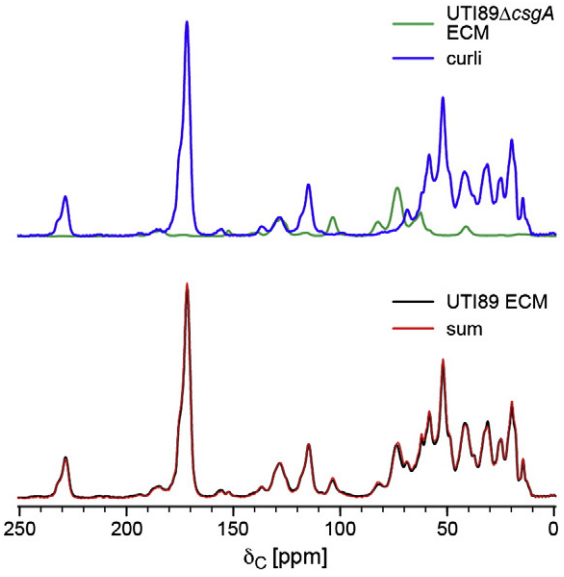

Fig. 5. Sum of the parts. The spectral sum of the UTI89Δ*csgA* extracellular material and purified curli (top) completely recapitulates the ^{13}C CPMAS spectrum of the intact UTI89 ECM. MAS was performed at 7143 Hz, and 32,768 scans were obtained for each spectrum.

contained 87% curli and 13% cellulose. As further confirmation that this scaling reveals an accurate estimate of curli and polysaccharide in the ECM, we also prepared a physical mixture of curli and the CR-containing UTI89Δ*csgA* ECM, harboring 75 mg and 25 mg of each, respectively, and obtained a similar spectrum to the UTI89 ECM spectrum (Fig. S2). Thus, the UTI89 ECM is approximately 85% curli and 15% cellulose.

Discussion

The genomics and proteomics revolutions have been enormously successful in generating full genome sequences for an increasing number of organisms and in predicting and determining the structures of a steadily increasing number of proteins. In essence, these data provide crucial "parts lists" for biological systems. Yet, formidable challenges exist in generating complete descriptions of how the parts function and assemble into macromolecular complexes and whole-cell assemblies. We have developed a quantitative "sum-of-the-parts" approach integrating electron microscopy, biochemistry, and solid-state NMR spectroscopy to examine the architecture and to determine the chemical and molecular composition of the bacterial ECM.

Electron microscopy experiments were invaluable in visualizing the architecture of the *E. coli* biofilms and the ECM, revealing macromolecular order at the single-cell level with individual bacteria being encapsulated in shell-like structures that join together to form extended structures. This architecture is maintained even after the use of fluid shear forces to mechanically separate the ECM from the cells. The lack of order exhibited by the curli mutant, UTI89 Δ*csgA*, suggests that the mechanical strength exhibited by the UTI89 ECM emerges from the interaction of curli and cellulose, consistent with recent discoveries that both components are required for biofilm formation at the air–liquid interface in UTI89 [20] and that increased curli production in the presence of cellulose enhances the strength, viscoelasticity, and resistance to strain of biofilms formed at the air–liquid interface [27,42]. Although electron microscopy allowed visualization of the curli-only sample, the curli mutant sample, and the important wild-type ECM, the separate images do not permit one to identify how much of each component is present in the intact UTI89 matrix.

As a noncrystalline, heterogeneous, and insoluble macromolecular assembly, analyses of the chemical composition of the ECM pose a challenge to most conventional methods of compositional analysis. Problems with quantification arise from the incomplete dissolution of the ECM as well as the uncertainty that results from enzymatic and chemical-digestion-induced changes. Solid-state NMR is non-perturbative and uniquely suited to provide compositional detail in such intact, complex systems. To dissect the contributions of curli and polysaccharides in the biofilm framework, we purified and obtained ^{13}C CPMAS spectra of (i) the wild-type UTI89 ECM, (ii) the curli-free ECM produced by the curli mutant strain UTI89Δ*csgA*, and (iii) purified curli. We discovered that a simple scaled sum of the curli and UTI89Δ*csgA* ECM spectra recapitulates the ^{13}C CPMAS spectrum of the UTI89 ECM. Every peak intensity and lineshape is matched in the scaled sum and UTI89 ECM spectra. Thus, although polysaccharides are often suggested as providing the matrix framework [43], we established that curli represent a significant fraction of the framework in the *E. coli* ECM, approximately 85% of the matrix by mass. Clearly, amyloid fibers and polysaccharides are co-produced in nature and form highly ordered supramolecular assemblies with unique mechanical and architectural properties. These architectures and compositional detail inspire the rational design and synthesis of new polymeric materials.

Our approach is powerful, versatile, and applicable to other biofilm systems. The analysis can be performed in the absence of bacterial mutants, as our spectra in Fig. 5 reveal that some protein and polysaccharide contributions can be resolved even with the resolution of the one-dimensional CPMAS spectra using non-isotopically enriched samples. Future work will investigate whether other biofilm formers similarly rely on such a small number of major biofilm components and whether the protein: polysaccharide ratio varies among organisms or as a

function of growth conditions or environmental stress, including treatment with biofilm inhibitors. As described above, conditions that upregulate curli production can enhance biofilm formation and biofilm strength and small-molecule inhibitors of curli production can prevent biofilm formation, yet methods to compare the overall protein and polysaccharide content and to assess other changes in composition in these intact systems have been elusive. The ability to define the composition of the ECM using solid-state NMR on the intact insoluble matrix material will be crucial in ongoing efforts to transform biofilm descriptors from vague terms such as glue and slime into chemically descriptive, quantitative parameters to correlate biofilm composition and function.

Materials and Methods

Strains and culture conditions

Non-isotopically labeled samples were prepared from UTI89, UTI89Δ*csgA*, and MC4100 grown on YESCA agar. Congo red was included (25 μg/mL) for the preparation of the ECM samples. The ^{15}N-labeled UTI89Δ*csgA* ECM sample was prepared from cells grown on a modified version of Neidhardt's Mops minimal medium agar [44] with the following final composition on a per liter basis: 20 g bacto agar; 8.372 g Mops; 1 g glucose; 717 mg Tricine; 508 mg NH_4Cl; 230 mg K_2HPO_4; 106.6 mg $MgCl_2$; 48 mg K_2SO_4; 30.2 mg guanine; 27 mg adenine; 22.4 mg uracil; 22.2 mg cytosine; 2.8 mg $FeSO_4{\cdot}7H_2O$; 73.5 μg $CaCl_2{\cdot}2H_2O$; 24.8 μg H_3BO_3; 16 μg $MnCl_2$; 7.2 μg $CoCl_2$; 3.6 μg $(NH_4)_6Mo_7O_{24}{\cdot}4H_2O$; 2.8 μg $ZnSO_4$; 2.4 μg $CuSO_4$; 2 μg each of thiamine, niacin, and pantothenic acid; 1 μg each of pyridoxine–HCl and riboflavin; and 0.1 μg each of biotin and folic acid, adjusted to pH 7.4 with KOH. For isotopic labeling, NH_4Cl was replaced with 98 atom% $^{15}NH_4Cl$ (Isotec). Plates and lids were dried fully in a sterile hood until no condensation was visible (~30 minutes) prior to inoculation by streaking from stock plates. Inoculated plates were incubated for 60 h at 26 °C in a refrigerated incubator set to continuously run the compressor thereby maintaining incubator humidity at or below 10% relative humidity as monitored by a Traceable Humidity-On-A-Card humidity indicator card (Control Company).

Transmission electron microscopy

Negative staining transmission electron microscopy was performed on cells and ECM samples that were harvested and washed in 10 mM Tris buffer and applied onto 300-mesh copper grids coated with Formvar film (Electron Microscopy Sciences, Hatfield, PA) for 2 min, rinsed in deionized H_2O, and negatively stained with 2% uranyl acetate for 90 s and dried. Samples were examined with the JEM-1400 (JEOL, LLC).

Scanning electron microscopy

Scanning electron microscopy was performed on bacteria grown on top of 0.2-mm-pore-size polycarbonate track-etched membranes on top of YESCA agar. Membrane-associated bacteria were fixed overnight in 2% glutaraldehyde and 4% paraformaldehyde in 0.1 M sodium cacodylate buffer (pH 7.3) at 4 °C and postfixed with 1% OsO_4 at 4 °C for 1 h. Samples were dehydrated in a series of increasing concentrations of ethanol (50%, 70%, 95%, and 100%), inserted into a critical point dryer, coated with gold-palladium, and visualized with a field emission scanning electron microscope (Zeiss, Sigma FEG-SEM).

ECM and curli purification

UTI89 ECM, UTI89Δ*csgA* ECM, and curli were purified utilizing a modified version of the curli extraction protocol of Chapman *et al.* [11]. Bacteria were harvested into 10 mM Tris buffer, pH 7.4, and sheared using an OmniMixer Homogenizer (Omni International) on ice (using motor setting 9) for five cycles of 1 min shear and 2 min rest. Cells were removed by centrifuging twice for 10 min at 5000*g*. For UTI89, the pelleted cells were subjected to a second round of shearing and centrifugation. Supernatants were spiked with 5 M NaCl to achieve a final concentration of 170 mM and pelleted for 1 h at 13,000*g*.

For non-SDS-washed ECM, pellets were resuspended in 10 mM Tris, pH 7.4, incubated overnight at 4 °C, and then pelleted, washed in Tris buffer, and pelleted again at 30,000*g* for 30 min. For SDS-washed ECM, pellets were resuspended in 10 mM Tris, pH 7.4, spiked with a 10% SDS stock to a final concentration of 4% SDS, and incubated, rocking at room temperature overnight. The ECM was then pelleted for 1 h at 13,000*g*, resuspended in Tris buffer, and pelleted at 30,000*g* for 30 min. The latter washing step was repeated until the SDS was removed. All pellets were resuspended in MQ water, flash frozen in liquid nitrogen, and lyophilized.

SDS-PAGE gels

Lyophilized samples were reconstituted in MQ water to give a concentration of 2 mg/mL. The desired quantity of material, between 2 and 150 μg, was distributed into individual 1.5-mL microcentrifuge tubes, frozen, and then lyophilized. The lyophilized samples were treated with 100 μL of 88% formic acid and vacuum centrifuged. The samples were reconstituted in 40 μL of SDS-PAGE sample buffer containing 8 M urea, centrifuged to remove insoluble material, and used for electrophoresis [45]. The gels were incubated for 10 min in 1.25 M Tris buffer, pH 8.8, to distinguish CR from Coomassie blue.

Solid-state NMR experiments

All solid-state NMR experiments were performed with an 89-mm wide-bore Varian/Agilent magnet at 11.7 T (499.11 MHz for ^{1}H, 125.49 MHz for ^{13}C, and 50.58 MHz for ^{15}N), Varian console, and a home-built four-frequency transmission-line probe with a 13.6-mm-long, 6-mm-inner-diameter sample coil and a Revolution NMR MAS Vespel stator. Samples were spun in thin-wall 5-mm-outer-diameter zirconia rotors (Revolution NMR, LLC) at 7143 ± 2 Hz, using a Varian MAS control unit. The temperature was maintained at 10 °C. π pulse lengths were 10 μs for ^{13}C and ^{15}N for both the

CPMAS [46] and REDOR [40] sequences. Proton-carbon matched cross-polarization transfers were at 50 kHz for 1.5 ms. Proton dipolar decoupling was employed at 83 kHz with TPPM modulation [47] and a 2-s recycle delay. The chemical shift scale of the ^{13}C NMR spectra was referenced to external adamantane. REDOR was used to restore the ^{13}C–^{15}N dipolar couplings that are removed by MAS [40]. REDOR experiments are always done in two parts, once with rotor-synchronized dephasing pulses (S) and once without (full echo, S_0). The dephasing pulses change the sign of the heteronuclear dipolar coupling, and this interferes with the spatial averaging resulting from the motion of the rotor. The difference in signal intensity (REDOR difference, $\Delta S = S_0 - S$) for the observed spin in the two parts of the REDOR experiment is directly related to the corresponding distance to the dephasing spin [40].

Acknowledgements

We thank the Cell Sciences Imaging Facility at Stanford (John J. Perrino) for assistance with electron microscopy. L.C. holds a Career Award at the Scientific Interface from the Burroughs Welcome Fund. We gratefully acknowledge support from the NIH Director's New Innovator Award (DP2OD007488), Stanford University, and the Stanford Terman Fellowship.

Supplementary Data

Supplementary data to this article can be found online at http://dx.doi.org/10.1016/j.jmb.2013.06.022

Received 3 April 2013;
Accepted 6 June 2013
Available online 1 July 2013

Keywords:
curli;
NMR;
functional amyloid;
biofilm;
extracellular matrix

† O.A.M. and X.Z. contributed equally to this work.

Abbreviations used:
ECM, extracellular matrix; CPMAS, cross-polarization magic-angle spinning; MAS, magic-angle spinning; REDOR, rotational-echo double-resonance.

References

[1] Costerton JW, Cheng KJ, Geesey GG, Ladd TI, Nickel JC, Dasgupta M, et al. Bacterial biofilms in nature and disease. Annu Rev Microbiol 1987;41:435–64.
[2] Flemming HC. Biofouling in water systems—cases, causes and countermeasures. Appl Microbiol Biotechnol 2002;59:629–40.
[3] Costerton JW, Lewandowski Z, Caldwell DE, Korber DR, Lappinscott HM. Microbial biofilms. Annu Rev Microbiol 1995;49:711–45.
[4] Hall-Stoodley L, Costerton JW, Stoodley P. Bacterial biofilms: from the natural environment to infectious diseases. Nat Rev Microbiol 2004;2:95–108.
[5] Cegelski L, Marshall GR, Eldridge GR, Hultgren SJ. The biology and future prospects of antivirulence therapies. Nat Rev Microbiol 2008;6:17–27.
[6] Donlan RM, Costerton JW. Biofilms: survival mechanisms of clinically relevant microorganisms. Clin Microbiol Rev 2002;15:167.
[7] del Pozo JL, Patel R. The challenge of treating biofilm-associated bacterial infections. Clin Pharmacol Ther 2007;82:204–9.
[8] Flemming HC, Wingender J. The biofilm matrix. Nat Rev Microbiol 2010;8:623–33.
[9] Sutherland IW. Biofilm exopolysaccharides: a strong and sticky framework. Microbiology 2001;147:3–9.
[10] Zogaj X, Nimtz M, Rohde M, Bokranz W, Romling U. The multicellular morphotypes of *Salmonella typhimurium* and *Escherichia coli* produce cellulose as the second component of the extracellular matrix. Mol Microbiol 2001;39:1452–63.
[11] Chapman MR, Robinson LS, Pinkner JS, Roth R, Heuser J, Hammar M, et al. Role of *Escherichia coli* curli operons in directing amyloid fiber formation. Science 2002;295:851–5.
[12] Alteri CJ, Xicohtencatl-Cortes J, Hess S, Caballero-Olin G, Giron JA, Friedman RL. *Mycobacterium tuberculosis* produces pili during human infection. Proc Natl Acad Sci USA 2007;104:5145–50.
[13] Capstick DS, Jomaa A, Hanke C, Ortega J, Elliot MA. Dual amyloid domains promote differential functioning of the chaplin proteins during *Streptomyces* aerial morphogenesis. Proc Natl Acad Sci USA 2011;108:9821–6.
[14] Dueholm MS, Petersen SV, Sonderkaer M, Larsen P, Christiansen G, Hein KL, et al. Functional amyloid in *Pseudomonas*. Mol Microbiol 2010;77:1009–20.
[15] Romero D, Aguilar C, Losick R, Kolter R. Amyloid fibers provide structural integrity to *Bacillus subtilis* biofilms. Proc Natl Acad Sci USA 2010;107:2230–4.
[16] Romling U, Sierralta WD, Eriksson K, Normark S. Multicellular and aggregative behaviour of *Salmonella typhimurium* strains is controlled by mutations in the agfD promoter. Mol Microbiol 1998;28:249–64.
[17] Larsen P, Nielsen JL, Otzenj D, Nielsen PH. Amyloid-like adhesins produced by floc-forming and filamentous bacteria in activated sludge. Appl Environ Microbiol 2008;74:1517–26.
[18] Larsen P, Nielsen JL, Dueholm MS, Wetzel R, Otzen D, Nielsen PH. Amyloid adhesins are abundant in natural biofilms. Environ Microbiol 2007;9:3077–90.
[19] Schwartz K, Syed AK, Stephenson RE, Rickard AH, Boles BR. Functional amyloids composed of phenol soluble modulins stabilize *Staphylococcus aureus* biofilms. PLoS Pathog 2012;8:e1002744.
[20] Cegelski L, Pinkner JS, Hammer ND, Cusumano CK, Hung CS, Chorell E, et al. Small-molecule inhibitors target *Escherichia coli* amyloid biogenesis and biofilm formation. Nat Chem Biol 2009;5:913–9.
[21] Anderson GG, Dodson KW, Hooton TM, Hultgren SJ. Intracellular bacterial communities of uropathogenic *Escherichia coli* in urinary tract pathogenesis. Trends Microbiol 2004;12:424–30.
[22] Kai-Larsen Y, Luthje P, Chromek M, Peters V, Wang X, Holm A, et al. Uropathogenic *Escherichia coli* modulates immune

responses and its curli fimbriae interact with the antimicrobial peptide LL-37. PLoS Pathog 2010;6:e1001010.
[23] Beloin C, Roux A, Ghigo JM. *Escherichia coli* biofilms. Bacterial Biofilms 2008;322:249–89.
[24] Schembri MA, Givskov M, Klemm P. An attractive surface: gram-negative bacterial biofilms. Sci STKE 2002;2002:re6.
[25] Zogaj X, Bokranz W, Nimtz M, Romling U. Production of cellulose and curli fimbriae by members of the family Enterobacteriaceae isolated from the human gastrointestinal tract. Infect Immun 2003;71:4151–8.
[26] Da Re S, Ghigo JM. A CsgD-independent pathway for cellulose production and biofilm formation in *Escherichia coli*. J Bacteriol 2006;188:3073–87.
[27] Lim JY, May JM, Cegelski L. Dimethyl sulfoxide and ethanol elicit increased amyloid biogenesis and amyloid-integrated biofilm formation in *Escherichia coli*. Appl Environ Microbiol 2012;78:3369–78.
[28] McCrate OA, Zhou X, Cegelski L. Curcumin as an amyloid-indicator dye in *E. coli*. Chem Commun 2013;49:4193–5.
[29] Toke O, Cegelski L. REDOR applications in biology: an overview. eMagRes. Chichester, UK: John Wiley & Sons, Ltd; 2007.
[30] Zhou XX, Cegelski L. Nutrient-dependent structural changes in *S. aureus* peptidoglycan revealed by solid-state NMR spectroscopy. Biochemistry 2012;51:8143–53.
[31] Cegelski L, Schaefer J. Glycine metabolism in intact leaves by in vivo 13C and 15N labeling. J Biol Chem 2005;280:39238–45.
[32] Kramer KJ, Hopkins TL, Schaefer J. Analysis of intractable biological samples by solids NMR. Nitrogen-containing macromolecules in the bio- and geosphere, 707. 1998. p. 14–33.
[33] Wood PJ, Fulcher RG. Interaction of some dyes with cereal beta-glucans. Cereal Chem 1978;55:952–66.
[34] Delcour AH, Zhou Y, Smith D, Hufnagel D, Chapman M. Experimental manipulation of the microbial functional amyloid called curli. Bacterial cell surfaces, Vol. 966. New York: Humana Press; 2013. p. 53–75.
[35] Lasserre JP, Beyne E, Pyndiah S, Lapaillerie D, Claverol S, Bonneu M. A complexomic study of *Escherichia coli* using two-dimensional blue native/SDS polyacrylamide gel electrophoresis. Electrophoresis 2006;27:3306–21.
[36] Vanderhart DL, Atalla RH. Studies of microstructure in native celluloses using solid-state C-13 NMR. Macromolecules 1984;17:1465–72.
[37] Kai A, Xu P, Horii F, Hu SH. CP/MAS C-13 NMR study on microbial cellulose fluorescent brightener complexes. Polymer 1994;35:75–9.
[38] Maunu S, Liitia T, Kauliomaki S, Hortling B, Sundquist J. C-13 CPMAS NMR investigations of cellulose polymorphs in different pulps. Cellulose 2000;7:147–59.
[39] Varki A. Essentials of glycobiology. Cold Spring Harbor, NY: Cold Spring Harbor Laboratory Press; 1999.
[40] Gullion T, Schaefer J. Rotational-echo double-resonance NMR. J Magn Reson 1989;81:196–200.
[41] Lindhorst TK, Kotter S, Krallmann-Wenzel U, Ehlers S. Trivalent alpha-D-mannoside clusters as inhibitors of type-1 fimbriae-mediated adhesion of *Escherichia coli*: structural variation and biotinylation. J Chem Soc Perkin Trans 2001;1:823–31.
[42] Wu C, Lim JY, Fuller GG, Cegelski L. Quantitative analysis of amyloid-integrated biofilms formed by uropathogenic *Escherichia coli* at the air–liquid interface. Biophys J 2012;103:464–71.
[43] Sutherland IW. The biofilm matrix—an immobilized but dynamic microbial environment. Trends Microbiol 2001;9:222–7.
[44] Fc Neidhard, Bloch PL, Smith DF. Culture medium for Enterobacteria. J Bacteriol 1974;119:736–47.
[45] Shewmaker F, McGlinchey RP, Thurber KR, McPhie P, Dyda F, Tycko R, et al. The functional curli amyloid is not based on in-register parallel beta-sheet structure. J Biol Chem 2009;284:25065–76.
[46] Schaefer J, Stejskal EO. C-13 nuclear magnetic-resonance of polymers spinning at magic angle. J Am Chem Soc 1976;98:1031–2.
[47] Bennett AE, Rienstra CM, Auger M, Lakshmi KV, Griffin RG. Heteronuclear decoupling in rotating solids. J Chem Phys 1995;103:6951–8.
[48] Serra DO, Richter AM, Klauck G, Mika F, Hengge R. Microanatomy at cellular resolution and spatial order of physiological differentiation in a bacterial biofilm. Mbio 2013;4(2), http://dx.doi.org/10.1128/mBio.00103-13.